International Journal of Applied Earth Observation and Geoinformation 122 (2023) 103424

Contents lists available at ScienceDirect

International Journal of Applied Earth Observation and Geoinformation

journal homepage: www.elsevier.com/locate/jag

Hydrocarbon production induced land deformation over Permian Basin; analysis using persistent scatterer interferometry and numerical modeling

Vamshi Karanam *, Zhong Lu

Southern Methodist University, Roy M. Huffington Department of Earth Sciences, Dallas, TX 75205, USA

ARTICLE INFO

Keywords:
Hydrocarbon extraction
Land deformation
Persistent scatterer interferometry
Saltwater disposal

ABSTRACT

The Permian Basin, encompassing Southeastern New Mexico and Western Texas, has been an important source of oil and natural gas for over a century for the United States. With recent advancements in petroleum extraction methods, such as hydraulic fracturing and horizontal drilling, production has increased exponentially. Such rapid developments, along with the disposal of wastewater back into the subsurface, have caused significant changes in the stress regime of the region's subsurface, resulting in various geohazards including land subsidence. In this work, we used the Sentinel-1C-band SAR dataset acquired between 2016 and 2021 to measure the basin-wide deformation over the entire Permian Basin. We utilized Persistent Scatterer Interferometry (PSI) technique to produce the time-series deformation at millimeter-level accuracy. The average monthly production and injection volumes and well depths over the Delaware Basin in New Mexico were calculated for each well and the impact of the hydrocarbon activities on the deformation was modeled using a distributed point source model from fluid volume and well depth data. The results show that the Permian Basin was deforming at a rate of 3–4 cm/yr., with two large pockets of deformation to the north of the Grisham Fault Zone (GFZ) in the Delaware Basin. The region south of the GFZ shows complex deformation features with linear patterns, indicating the presence of faults hindering fluid flow. Some areas in the Delaware Basin also show an uplift, especially along the Texas side of the border driven by shallow wastewater injection. The Midland Basin is also affected by subsidence with several localized subsidence zones identified in the region. Further, the Midland Basin experienced an increase in intensity and the spatial distribution of the deformation over the last few years. Given both production and injection well data, the modeled deformation results agree with the observed except in two pockets. When only production data is used for the modeling, the modeled deformation shows better agreement with the observed, especially in the interior of New Mexico. The modeling results suggest that the deep wastewater injection has minimal impact on surface deformation in the region. Additionally, it is also possible that the region has undergone inelastic deformation. While we used an elastic model in this preliminary study, a more accurate study requires regional poroelastic modeling to study the interaction between the solid subsurface and fluid hydrocarbons in detail.

1. Introduction

Since the advent of commercial petroleum extraction methods, petroleum, and its products have become ubiquitous across the globe. As its importance grew, more and more exploration operations have been conducted to identify commercially viable petroleum deposits. Simultaneously, new techniques have emerged in the field of petroleum extraction to efficiently exploit the hydrocarbon reserves. Over the last few decades, the increasing exploration of hydrocarbons has contributed to the alarming increase in geohazards, sometimes permanently altering the local ecosystem, and is a growing concern for communities and policymakers worldwide (Dhakal et al., 2022; Frohlich et al., 2016; Jones et al., 2015). To ensure that the benefits of hydrocarbon production are realized efficiently, it is important to understand the dynamics of the geohazards at various stages in production.

Permian Basin, located along the borders of New Mexico and Texas has huge hydrocarbon reserves accounting for more than 40% of the oil production in the United States (Popova & Long, 2022). Permian Basin is composed of 3 major subbasins: Delaware Basin, Central Basin Platform, and Midland Basin. The recent advancements in extraction techniques

* Corresponding author.
E-mail address: vkaranam@smu.edu (V. Karanam).

https://doi.org/10.1016/j.jag.2023.103424
Received 12 May 2023; Received in revised form 22 June 2023; Accepted 13 July 2023

such as hydraulic fracturing and horizontal drilling have accelerated the productivity of shale gas rapidly over the past two decades. The hydrocarbon production and the associated wastewater disposal alter the stress regime in the subsurface, resulting in surface deformation, possible activation of faults, and leakage of wastewater and hydrocarbons into the nearby aquifers and air that can impact the region's infrastructure and ecosystem (J. W. Kim & Lu, 2018; Savvaidis et al., 2020; Snee & Zoback, 2018; Zhai et al., 2021). The faults can act as barrier-conduit systems to modify the subsurface fluid flow that can be reflected in the surface deformation patterns (Bense & Person, 2006; Lu & Danskin, 2001).

Land subsidence largely goes unnoticed, especially in sparsely inhabited regions like the Permian Basin due to its relatively slow movement and large spatial extent. However, this can cause major damage to the pipelines, transportation, and other infrastructure in the region. Terrestrial techniques like leveling and total station provide accurate monitoring but are labor-intensive and time-consuming. GPS monitoring requires stations to be set up and have a coarse spatial resolution. Surface deformation can be estimated using the satellite Interferometric Synthetic Aperture Radar (InSAR) techniques over large spatial scales at fine spatial and temporal resolutions (e.g., Lu and Dzurisin, 2014). Advanced time-series InSAR techniques make use of Persistent Scatterers (PS) and Distributed Scatterers (DS) to provide temporal deformation trends with up to millimeter-level precision (Ferretti et al., 2011; A. J. Hooper, 2008). InSAR can be used to monitor a wide range of geohazards such as subsidence, volcanoes, earthquakes, and landslides (Drouin & Sigmundsson, 2019; Joshi et al., 2023; Kandregula et al., 2022; Karanam et al., 2021; J. Kim et al., 2022). InSAR has also been successfully used to monitor the oil production-induced deformation in the Permian Basin (Staniewicz et al., 2020), Lost Hills oilfield in California, US (Shi et al., 2022), Groningen gas field, Netherlands (Ketelaar, 2009), and Yellow River delta, China (Liu et al., 2016). The Lost Hills oilfield deformation was modeled using regression models, assuming the injection and production volumes are independent variables. Further, InSAR can provide data to constrain fault slips (Qu et al., 2019; Wright et al., 2001).

Zheng et al. (2019), with the help of finite element modeling, have discussed the leakages in wastewater injection wells inferred from surface uplift observations. Kim et al. (2019) monitored sinkholes near Wink in West Texas using TerraSAR-X imagery and concluded that although the existing sinkholes have stabilized, the residual subsidence continues. They have also identified a rapidly subsiding region possibly induced by severe drought in 2011 hinting at the formation of another sinkhole. Staniewicz et al. (2020) with the help of InSAR, estimated the deformation between 2014 and 2019 covering most of the Delaware Basin using SBAS techniques. They concluded that fault slip driven by petroleum operations is one of the major mechanisms leading to surface subsidence. Zhai et al. (2021) showed that most seismic activity in the Delaware Basin in West Texas is driven by shallow wastewater injection. Pepin et al. (2022) have used 2D and 3D edge dislocation models to show that the deformation in the southern part of the Delaware Basin is driven by seismic activity along normal faults induced by wastewater injection near critically stressed normal faults. However, this study did not consider the contribution of petroleum operations to surface deformation. Further, to the authors' knowledge, aseismic deformation in the northern part of the Delaware Basin in New Mexico where earthquakes are rare was not studied before. In this region, the deformation patterns do not represent any fault slips and therefore, the conclusions from the studies cannot be applied to this region. The increasing hydrocarbon activities and associated earthquakes in the other parts of the Permian Basin, especially the Central Basin Platform and the Midland Basin, necessitate a comprehensive study of the entire basin (Savvaidis, 2021; USEIA, 2023).

The objective of the study is to map the surface deformation over the entire basin and quantify the relation between the hydrocarbon operations and the surface deformation. We produced the time series deformation maps over the three major sub-basins of the Permian Basin from 2016 to 2021 using the PS InSAR analysis. We discussed the impact of hydrocarbon extraction activities and the faults on surface deformation. We used distributed point source model for understanding the relationship between the deformation and the petroleum extraction and injection activities in the northern Delaware Basin.

2. Study area

The Permian basin is a geologic depositional and structural basin, spreading across a 200,000 km^2 area in Southeastern New Mexico and West Texas. The area is known for its hydrocarbon reserves and has been actively exploited for over a century. The region is sparsely vegetated with a few cities scattered over the region, and much of the study area is used for hydrocarbon production. The Permian basin is a sedimentary basin that is eventually divided into three major sub-basins due to its asymmetrical development. The Central Basin is an elevated platform that separates the Delaware and Midland Basins (Fig. 1) (Horne et al., 2021). The sediment deposition took place between the Precambrian and Pennsylvanian periods. The three basins, at large, have different geological structures.

Hydrocarbon production started in the Delaware Basin in the early 1900 s and peaked in 1970 using conventional techniques. Due to the decline in conventional hydrocarbon reserves, production declined slowly until unconventional techniques such as hydraulic fracturing and horizontal drilling boosted production to new highs. Much of the production has been happening in the Delaware Basin and the Midland Basin.

The Delaware Basin is divided into several geologic layers characterized by depositional types and time periods (Popova, 2020b). Wolfcamp formation is an organic-rich formation deposited during Pennsylvanian and Wolfcampian times and spread across the three sub-basins. This formation is subdivided into four sections (A, B, C, and D with increasing depths) considering lithology and porosity among other parameters. The permeability of the Wolfcamp Formation is low due to the tight shale formations while the porosity averages around 6%. The Bone Spring Formation sits above the Wolfcamp Formation with the deposition of calcareous, siliciclastic, and carbonaceous marine deposits belonging to the Leonardian period. This formation has been the major producer of oil using conventional techniques for a long time. The Bone Spring Formation is further divided into four sections with alternating carbonate and sand layers. The Delaware Mountain Group (DMG) at the top consists of sandstones and organic-rich siltstones. The formation developed during the Guadalupian time. The DMG is further divided into Bell Canyon, Cherry Canyon, and Brushy Canyon. The Grisham Fault Zone (GFZ), a strike-slip system, runs west to east in the middle of the Basin and is home to a complex wrench fault system (Hennings et al., 2021; Horne et al., 2021).

In the Midland Basin, the Spraberry Formation overlies the Wolfcamp Formation (Popova, 2020a). It is composed of siltstones, sandstones, mudstones, and limestones. The formation is divided into lower, middle, and upper Spraberry sections. Historically, this formation has been uneconomical due to its low permeability. Recently it has been developed as an unconventional production zone. However, there are currently no regional surface deformation studies over this region. The recent surge in the occurrence of strong earthquakes in the Midland Basin (e.g., M 5.4 earthquake near Midland, Texas on Dec 16, 2022) emphasizes the need for a detailed study of geohazards in the region.

3. Datasets and methodology

3.1. InSAR analysis

The evolution of surface deformation between 2016 and 2021 is estimated using advanced InSAR processing of Sentinel-1 A/B (C band) datasets using the StaMPS technique (A. J. Hooper, 2008). The Sentinel-

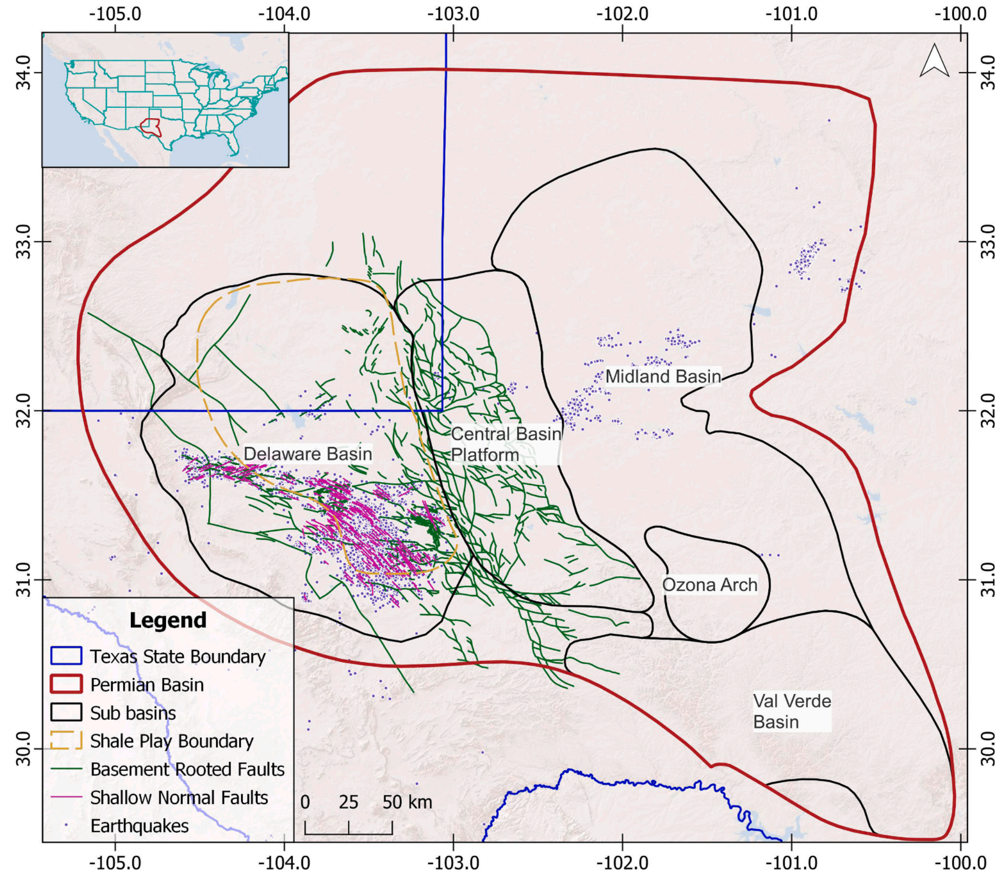

Fig. 1. Faults and,earthquake locations over the Permian Basin.

1A/B data are available for free download from Alaska Satellite Facility (Data, 2016). Three ascending tracks are required to cover the study area entirely. The descending data is only available for one track that partially covers the Permian Basin and was used for validation of the results from ascending track and estimation of 2D (vertical, east–west) deformation components from two different looking directions. The details of the datasets are tabulated below (Table 1). The Permian Basin is mostly a flat barren land devoid of vegetation. The coherence, therefore, is high in InSAR pairs with large temporal baselines. Thus, the PS technique which relies on the coherent pixels above a minimum threshold known as PS points is chosen for the study (Crosetto et al., 2016; A. Hooper et al., 2004; A. J. Hooper, 2008). The PS points are the stable scatterers with high and relatively stable reflectivity like buildings, barren land, and oil well machinery which can provide more reliable estimates of the ground motion at a good resolution. Finally, we generated the 2D (vertical d_{ver} and east–west d_{ew}) time series surface deformation maps over the entire basin (Eq. (1) (Garg et al., 2022). To obtain true 3D displacements, we need at least 3 independent observations (Zheng et al., 2023). However, we only have two independent observations available in ascending and descending directions. This makes it an ill-posed inverse problem. Meanwhile, InSAR is sensitive to the displacement in the flight direction which is close to North-South (Mishra and Jain, 2022). Therefore, it is a generally assumed that the N-S displacement is absent from the observations to obtain a unique solution for vertical and east–west deformations. Further, we have ignored the east–west deformation in the areas covered by only the ascending data to avoid the underdetermined case, considering that the deformation due to fluid extraction is primarily vertical. While the associated horizontal deformation can still be present in this region, it is expected to be very small compared to the vertical deformation and is in response to vertical deformation (e.g., as the surface moves up, the points move closer) and therefore is not significant. All data processing was completed using the High-Performance Computing (HPC) infrastructure at Southern Methodist University (SMU) as detailed in the figure below (Fig. 2).

$$\begin{matrix} d_{asc} \\ d_{des} \end{matrix} = \begin{pmatrix} \cos\theta_{asc} & -\cos\alpha_{asc}\sin\theta_{asc} \\ \cos\theta_{des} & -\cos\alpha_{des}\sin\theta_{des} \end{pmatrix} \begin{pmatrix} d_{ver} \\ d_{ew} \end{pmatrix} \quad (1)$$

Where d_{asc} and d_{des} are the deformations from ascending and descending tracks, respectively, θ is the incidence angle and α is the satellite heading angle.

The SLC images are mosaiced, co-registered, and single reference interferograms were generated. An amplitude dispersion index of 0.4 is chosen for the selection of PS points. A few interferograms severely contaminated with tropospheric errors are dropped to ensure reliable results. Then we filled the area with no PS points using interpolation assuming that the deformation is spatially continuous. Finally, the PSI results were validated using GPS observations obtained from the Nevada Geodetic Laboratory of the University of Nevada, Reno (Blewitt et al., 2018). However, not all the GPS stations match the study period (2016 –

Table 1
InSAR data used for the analysis.

Path	Number of datasets (After mosaicking)	Time period	Satellite direction
5	136	Oct 2016 to Dec 2021	Ascending
78	145	April 2016 to Dec 2021	Ascending
151	145	Oct 2016 to Dec 2021	Ascending
85	132	Jan 2016 to Dec 2021	Descending

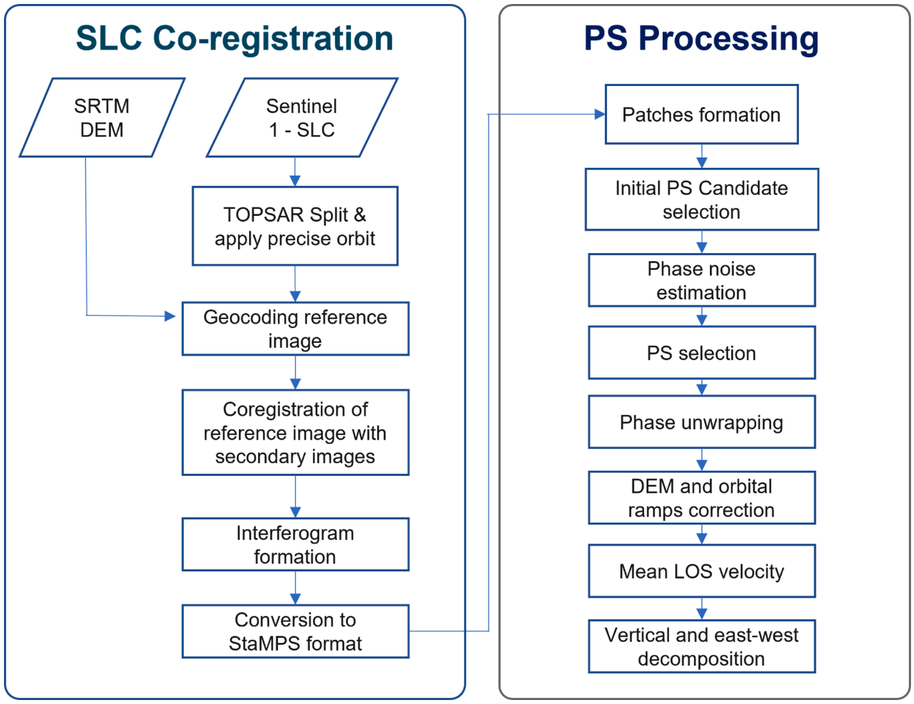

Fig. 2. Processing workflow for PSI analysis.

2021) and very few GPS stations are located over the deforming regions. The time period of the dataset was divided into two parts to understand the effect of the sharp increase in hydrocarbon extraction after 2018 on surface deformation while ensuring good coherence.

3.2. Modeling the injection and extraction volumes

The study area is spanned across two states, New Mexico, and Texas. In Texas, the production and injection volume data are maintained by the Railroad Commission of Texas (RRC); in New Mexico, the information is released by the New Mexico Energy, Minerals, and Natural Resources Department (EMNRD). Monthly production and injection volumes, well locations, and well depths are obtained. Then, the average monthly production and injection volumes are calculated. The stratigraphic layers, shallow normal fault maps, and the basement rooted fault maps are obtained from the US Energy Information Administration (EIA) and the Bureau of Economic Geology (BEG), UT Austin database (Hennings et al., 2021; Horne et al., 2021). The dataset contains formation depth maps and isopach maps for seven geologic layers in the Delaware Basin and Midland Basin. Earthquake data is obtained from the TexNet high-resolution catalog (Savvaidis, 2021). The data is used to correlate with the land subsidence patterns in the study region.

The subsurface is composed of porous media and the interaction between these porous solids and the hydrocarbons in a fluid state will reduce the effective stress on the system due to the introduction of the pore fluid pressure. In addition, the varying geology in depth across the study area requires complex modeling methods. But such modeling methods consume significant time, computation power, and labor. The presence of thousands of wells with time-varying fluid exchange influencing the deformation will further increase the complexity of the model. However, simpler models with a defined set of assumptions are computationally efficient, can reproduce the observations to the first order, and provide a generalized understanding of the processes. In addition, simple models can be useful for testing the hypothesis and exploring the relationship between the hydrocarbon operations and the surface deformation, helping to identify key assumptions and variables that need to be included in the complex models. In this study, the distributed point source model is used for the forward modeling of subsidence in the northern Delaware Basin region. We have used the average production and injection volume along with the 3D well locations to model the deformation at each well. The production volume includes both the oil and produced water. A 10*10 km^2 area with a grid spacing of 0.5*0.5 km^2 with the well in the center is assumed and the deformation at each point induced by the extraction and injection operations at the well is modeled. Then, using the principle of superposition, deformation induced by different wells is added to generate a cumulative surface deformation map. The model assumes a homogeneous and isotropic point source and estimates the surface deformation at a distance, induced by the pressure changes at the source. While this is a simplified model in the geological sense, considering that most of the wells fall in the bone spring formation, and the stratigraphy gradient in the deformation zones is low, this model can provide an important first order understanding of the relation between the fluid extraction/injection and the surface deformation. To obtain the displacement u_x, u_y, u_z induced on a point at a location (x,y) with the hydrocarbon well at a depth d (x_0, y_0 and d) is given as

$$\begin{pmatrix} u_x \\ u_y \\ u_z \end{pmatrix} = \beta \Delta V \frac{(1-\nu)}{\pi R^3} \begin{pmatrix} x - x_0 \\ y - y_0 \\ d \end{pmatrix} \tag{2}$$

where R is the radial distance ($R = \sqrt{(x-x_0)^2 + (y-y_0)^2 + d^2}$) from the source to the point on the surface. ΔV is the injection volume, ν is the Poisson's ratio (Mogi, 1958; Zheng et al., 2019). Here, a poroelasticity constant, β is introduced to account for the material properties and the source strength of the subsurface (Lu et al., 2002). The primary analysis was carried out on the dataset between 2018 and 2021 and the resulting model was tested on the 2016–2017 dataset.

4. Results

The Permian Basin is an important hub for hydrocarbon production. Currently, more than 5.6 million BBL (0.89 million m^3) of oil, and more than 2.2 million MCF (0.64 million m^3) of gas are produced from the basin every day (USEIA, 2023). Production increased over the last few years with the introduction of unconventional production techniques.

Hydrocarbon production was at a constant rate per year until around 2010 and then doubled in the next 6–7 years (Fig. 3). Between 2017 and 2018, oil production increased rapidly. In New Mexico, oil production increased by nearly three times between 2018 and 2020. Figure S1 shows the PS density for the deformation map over the Permian Basin obtained using StaMPS technique. These results were interpolated to fill the no data points to produce final deformation map (Fig. 4). The rapid changes in production are reflected in the observed surface deformation, especially over the Delaware Basin (Fig. S2). Further, most of the injection has been happening along the borders on the Texas side of the Texas-New Mexico border in the Delaware Basin and in the Central Basin Platform (Fig. S3). However, the Central Basin is largely unaffected by the deformation except for a few localized deformation zones mainly showing the uplift induced by the injection activities. While the geology of the Delaware Basin is different from that of the Central Basin, further investigation into the basin's stratigraphy and the injecting formations is required. Meanwhile, oil production in the Midland Basin increased significantly after 2018 with production and injection wells scattered around the central part of the Midland Basin.

The shale play region in the Delaware Basin is subsiding at an average rate of 3–4 cm/yr, with several large pockets of deformation. Overall, the subsidence in the region has grown in intensity and spatially after 2018 in line with the production in the region. The two regions with significant growth in the intensity and spread of the deformation are the Northern Delaware Basin and the Southern Midland Basin (Fig. 4). The deformation results are decomposed into vertical and east–west components over the areas with overlapping ascending and descending tracks that cover the entire Delaware Basin. The decomposed results show that most of the deformation is vertical with a small east–west component, especially along the faults in the Delaware Basin (Fig S4). Due to lack of overlapping tracks in the descending direction, the vertical deformation maps for the other two subbasins could not be produced. Considering that the factors triggering the deformation are the same across the Permian Basin, we assumed that the deformation is primarily vertical across the basin and vertical deformation maps for the other two basins were estimated. The principal focus of the study is to understand the deformation patterns at a regional level and thus, localized deformation signals are ignored. The time-series results from InSAR observations were compared to the GPS observations to validate the results. GPS station TXP6 is close to a deformation bowl in south Texas. The station was active only for the year 2021. However, the GPS observations match the InSAR results during the overlap period. Observations from the TXSO station over Midland Basin cover the entire study period and show seasonal deformation patterns that match with the InSAR results (Fig. 4). Taking the increase in the hydrocarbon production after 2018 into account, we have divided the time-series results into before (2016–2017) and after (2018–2021) the increase (Fig. 5). A stripe running through the middle of the study area is visible in Fig. 5 (a) because the data is from two different tracks each partially covering the study area. The area to the left of the stripe is from the track 151 and the area to the right is from the track 78. The discontinuity is expected due to the difference in incidence angle for the near range and far range. While we decomposed the data to vertical components to minimize the effect of the radar geometry, it could not be completely eliminated from the small section in data from 2016 to 17. This could be due to the presence of small tropospheric artefacts which could not be removed using the available techniques.

4.1. Delaware Basin

The InSAR results between 2016 and 2017 show that the northern Delaware Basin is largely unaffected by the deformation. A few localized subsidence zones caused by potash mining can be observed in the New Mexico part of the Delaware Basin. Further, the Delaware Basin is also affected by the uplift, especially along the borders of Texas and New Mexico induced by shallow wastewater injection. Figure S4 shows the east–west deformation over the Delaware Basin.

In the north-west part of the Delaware Basin, we observe an uplift of ∼ 10 mm/yr. This intriguing signal is consistent over the years. The deformation rate increases from west to east until it reaches the shale play boundary. The same deformation pattern can also be seen in the 2018–2021 results. This regional uplift is not directly related to the hydrocarbon operations as the hydrocarbon activities in the region are limited. While a sound geophysical explanation for the uplift requires a detailed understanding of the faulting and stratigraphy in the region and the use of complex modelling methods, it is possible that the fluid pressure from the injected fluids in New Mexico was diffused southward over a large area and is manifested as a regional long-wavelength uplift observed in the Western Delaware Basin. Meanwhile, hydrocarbon extraction of many decades in the region may induce long-wavelength surface rebound due to unloading. The observed long-wavelength uplift is a remarkably interesting case of surface deformation and further studies are required to understand the mechanisms of this deformation signal.

Most of the deformation in the south-west part of the Delaware Basin is up to −4 mm/yr except for two pockets where the deformation reaches −7 mm/yr. The region hosts the Davis Mountain range. Vegetation, varying surface type and geometry, and fluctuating atmosphere of the

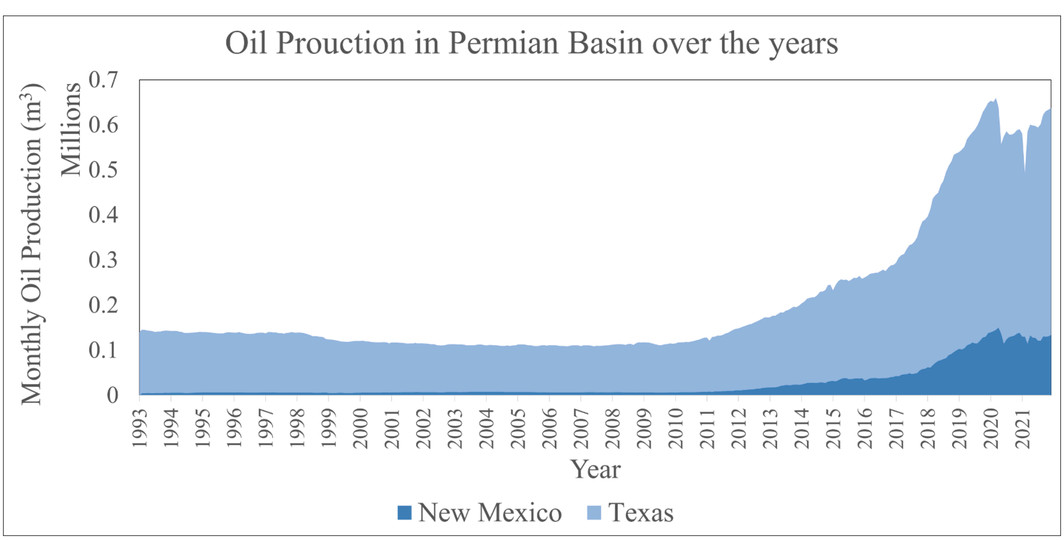

Fig. 3. Oil production over the years in Permian Basin.

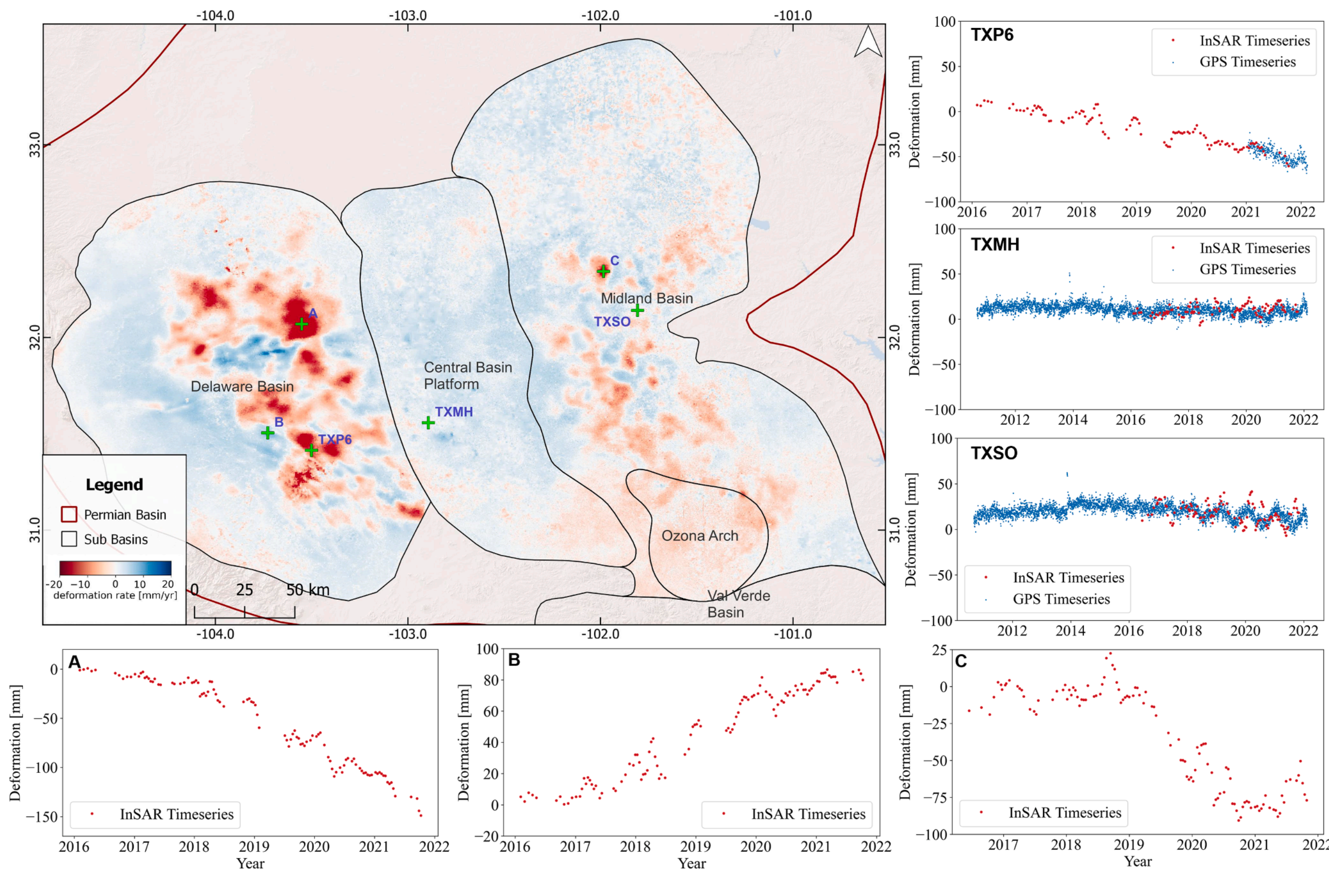

Fig. 4. Average vertical deformation rate map of the Permian basin with deformation time series over a few points.

mountains can introduce errors in the InSAR results, and it is possible that the residual topography-correlated tropospheric artifacts exist in the final deformation results. We tried correcting the results for the tropospheric error by removing the contaminated interferograms from the dataset followed by applying the tropospheric error correction (Bekaert et al., 2015a, 2015b; Yu et al., 2018). Even after implementing the corrections, the signal in question persisted. An important thing to consider is that the signal is also present in the 2018–2021 dataset, although at a lower magnitude. Considering that the mountains are far from the oil fields, we do not expect to observe any subsidence related to hydrocarbon production in the region. It is also possible that the observed signal represents the deformation in the region induced by sources not related to hydrocarbon production.

Further, the region north of the GFZ primarily shows deformation increasing radially outwards while the region to the south of GFZ shows complex deformation patterns with linear patterns indicating the presence of faults. The area surrounding Pecos City in the Delaware Basin is undergoing differential settlements with uplift on one side and subsidence on the other side. The potash mining-induced subsidence zones show a decreasing trend in intensity and spatial extent over the last few years due to the reduction in mining activities. Zhang et al. (2018) have explored the mining deformation in detail. The mining-induced subsidence was at 100 cm/yr between 2007 and 2011, while during the current study period, the subsidence is reduced to 4 cm/yr. Oversupply of Potash in the international market especially from countries like Canada, China and Russia over the last decade has impacted the Potash prices which led to decline in the Potash production in the region (Intrepid Potash, 2016; Zhang et al., 2018). Therefore, several mines were abandoned with no further mining activities resulting in stabilization of surface. Meanwhile, room and pillar technique are used in the mining here which involves leaving out some portions of the ore as support for the overburden. These pillars may fail due to aging or salt dissolution may occur due to freshwater leakage or impoundments. The subsidence induced by such factors can continue for longer even after a mine is abandoned. However, considering that the current study focuses on regional subsidence features, and it is possible that localized deformation signals may require more processing for troposphere and other error removal. In total, close to 13,000 sq km area was estimated to be deforming in the Delaware Basin. Though there is a basement-rooted fault between the two deformation centers in New Mexico, the deformation seems to have not been influenced by the fault considering that the injection and extraction depths are shallower than the fault depth.

4.2. Midland Basin

Midland Basin has become increasingly important for hydrocarbon production over the last few years resulting in surface deformation. The deformation patterns in the Midland Basin are distinct from those of the Delaware Basin. While the deformation in the Delaware Basin is spread over a large area, several localized deformation patterns can be observed in the Midland Basin. The subsidence and uplift are intertwined in the region. In addition, the intensity of the deformation is much lower in the Midland Basin compared to Delaware Basin at 1–2 cm/yr. This difference between the Delaware Basin and Midland Basin can be because Delaware Basin has been experiencing surface deformation for much longer than the Midland Basin and thus, the smaller deformation zones are merged over time, while in Midland Basin, they are still distinct. The deformation in the Midland Basin extends towards the south to Ozona Arch. The northern part of the basin is largely occupied by agricultural lands and petroleum production is limited here. The coherence is low over the agricultural lands and therefore, the PS points are limited (Fig. S1). Further, several groundwater extraction wells are located over the agricultural lands in the Northern Midland Basin and no deformation has been observed here from our results. In total, 3240 sq km subsidence and 3040 sq km uplift are observed. Between 2016 and 2021, several new deformation centers emerged. The recent earthquakes in the Midland Basin on Dec 16, 2022 (5.4 M at 9 km depth in Midland) and Nov 16, 2022 (5.4 M at 6 km depth in Mentone), also add to the importance of studying the impact of hydrocarbon operations on the subsurface in the Midland Basin. However, modeling the surface

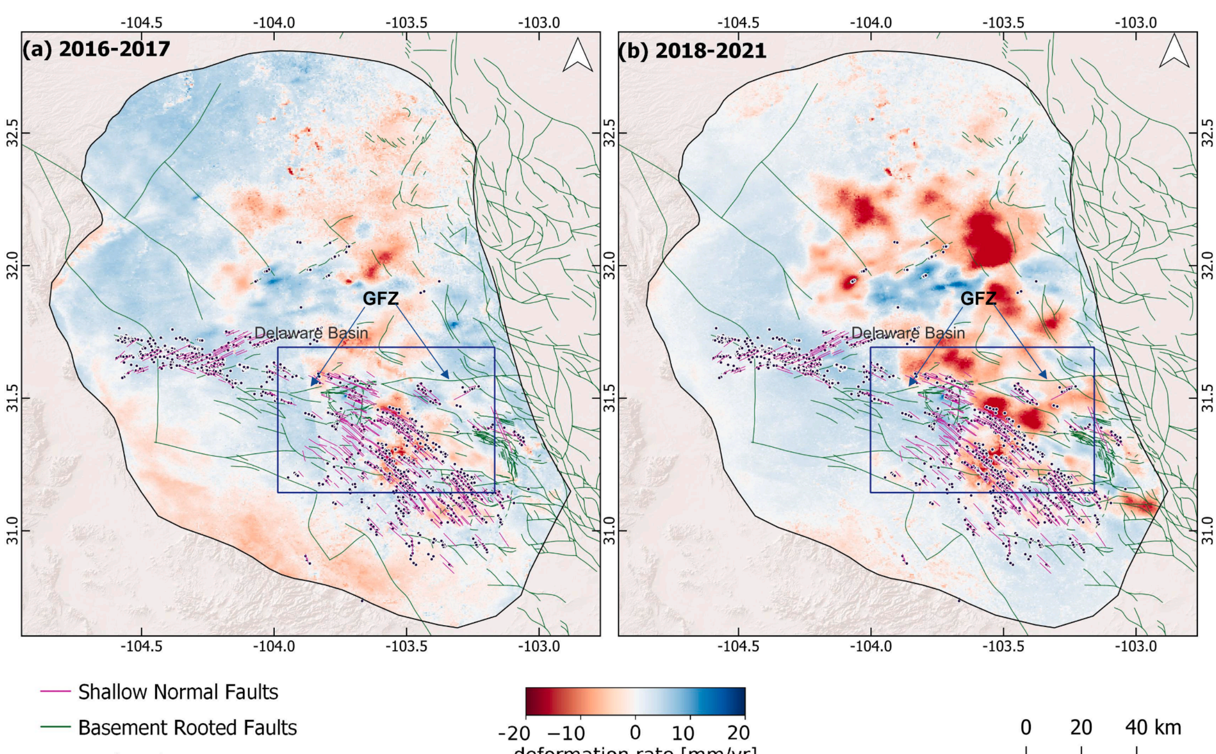

Fig. 5. Average deformation velocity map of the Delaware sub-basin for the time periods (a) 2016–2017 (b) 2018–2021.

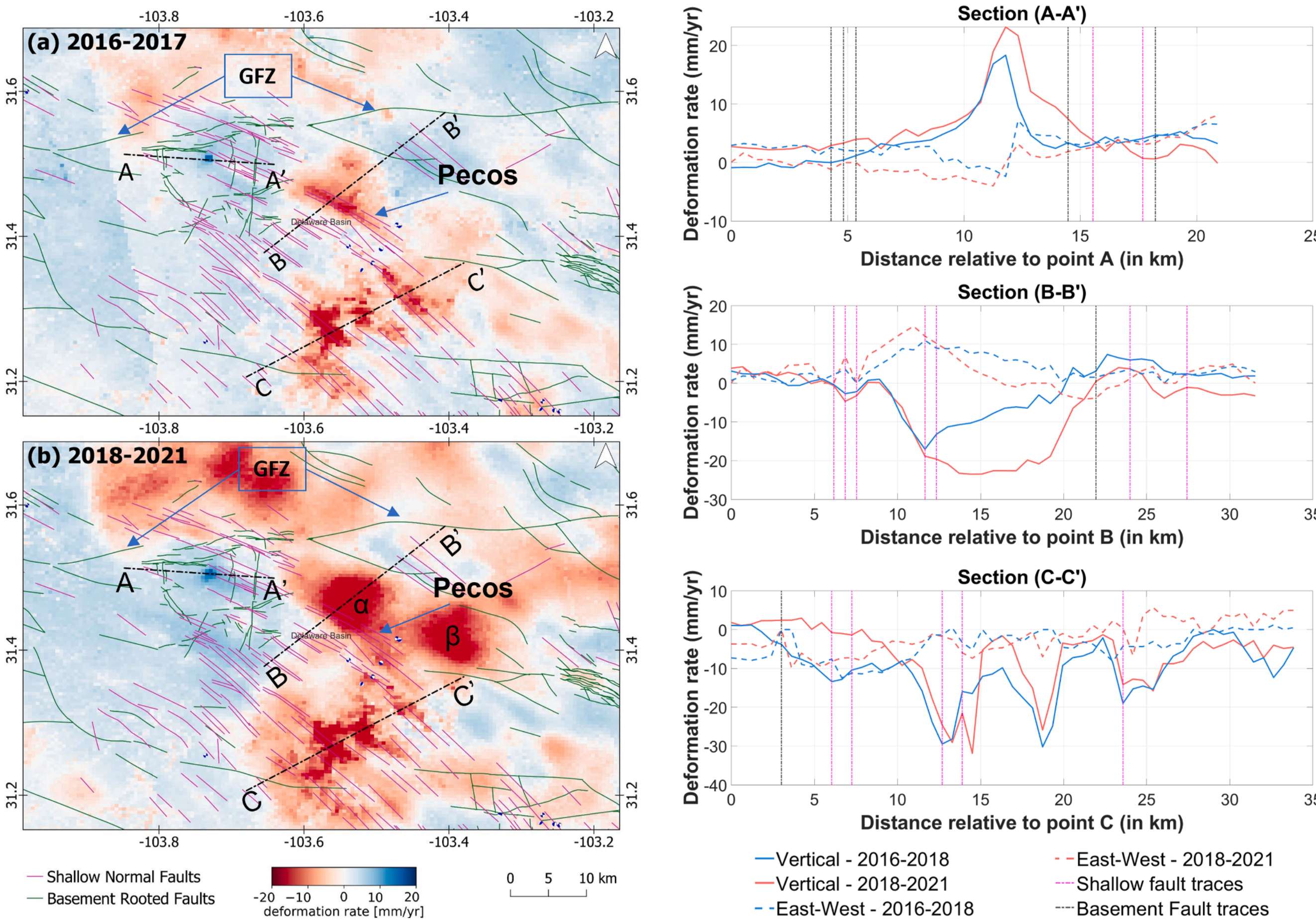

Fig. 6. Influence of interaction between faults and hydrocarbon fluids on the surface deformation in the southern Delaware Basin area (the area inside the box in Fig. 5) between (a) 2016–2017 and (b) 2018–2021.

deformation in the Midland Basin is tricky due to the presence of several localized subsidence zones and thousands of hydrocarbon wells requiring the geology and stratigraphy data at a very high resolution, thereby making the modeling computationally costly and labor intensive. Further, any complex subsurface features such as faults and underground tunnels increase the complexity of the modeling.

4.3. Central Basin

The Central Basin is largely unaffected by the deformation. Still, a few small and localized uplift zones have emerged in the last few years. Hydrocarbon production is limited in the Central Basin. However, there was a significant amount of injection along the borders of the Central Basin Platform. The injection activities did not produce any deformation of the same level in comparison to the other Basins. Kim et al. (2019) have discussed the evolution of the sinkholes in the Central Basin Platform near Wink, Texas subsiding at a rate of ~ 50 cm/yr during 2007–2011 close to the previously collapsed sinkholes observed using the very high-resolution TerraSAR-X imagery. Even though the spatial extent of the sinkholes is small, such events can cause major damage to the pipelines and the transportation infrastructure. Considering the spatial resolution chosen for the current study, while such localized deformation is still observed, their intensity may be underestimated.

5. Discussion

5.1. Influence of faults on the surface deformation

A rock is expected to fail when the shear stress exceeds a threshold. Mathematically, it is expressed as $\tau_{crit} = \mu(\sigma_n\text{-P}) + \tau_0$, where τ_{crit} is the critical shear stress, μ is the coefficient of friction, σ_n is the normal stress and P is the pore pressure and τ_0 is the cohesive strength of the sliding surface (Ellsworth, 2013). Wastewater injection increases the pore pressure in the rock. This reduces the critical shear stress required to initiate failure. The fault slips influence surface deformation, resulting in a differential settlement on either side of the fault plane (Pepin et al., 2022). In addition, the faults may act as barrier-conduit systems for the fluid flow, due to the contrasts in hydromechanical properties, such as permeability, between and within the components, the orientation of the fault, fault width, stress changes, grain reorganization, etc. resulting in differential subsidence on either side of the fault (Bense & Person, 2006; Lu and Danskin, 2001; Caine & Forster, 1999). Previous studies have experimentally shown that the pressure changes due to the injection on the same side of a nearby fault can be significantly different from those on the other side of the fault (Denlinger et al., 2020). The stress accumulated over time gets released suddenly, initiating fault slips accompanied by differential settlements. Quantification of this possible effect will require an extensive understanding of the interplay of the stress regime, the faults, and the geology of the region.

The deformation profiles in the Southern Delaware Basin show complex patterns. The most interesting example of the effect of faults on the deformation can be seen from section profile A-A' where a localized uplift region is surrounded by the faults on all four sides with a stable spatial extent over the years between 2016 and 2021 (Fig. 6). Here the injection formation is covered by faults on all four sides. The shallow normal fault traces and the basement rooted fault traces along the profile are plotted as vertical lines on the graph. In section B-B', the presence of faults may have restricted the deformation to the eastern side of the fault

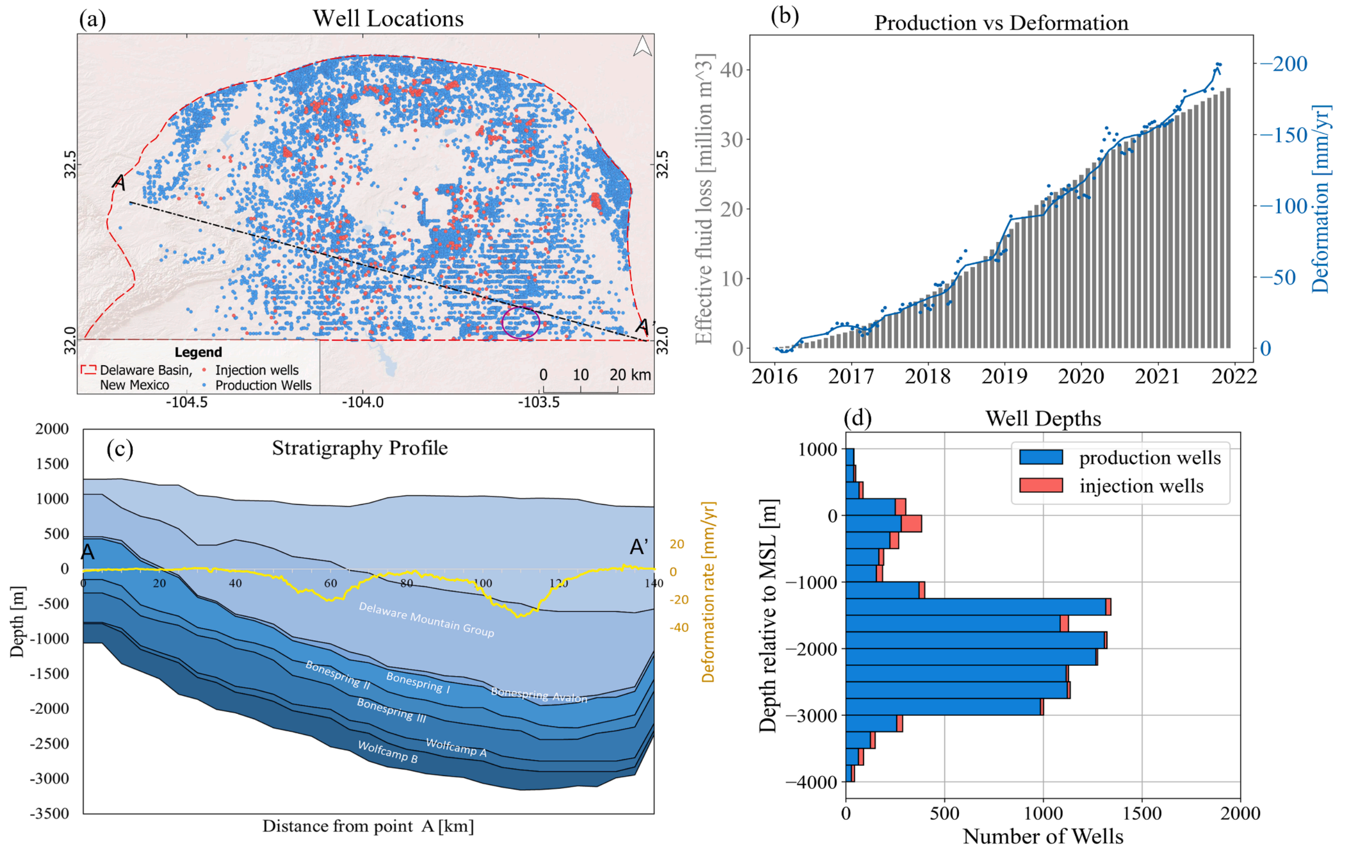

Fig. 7. (a) The distribution of the production and injection wells in the Northern Delaware Basin, New Mexico (b) Correlation between the cumulative hydrocarbon production and the deformation over the region highlighted in Fig. 8-a (c) section profile A-A' of the stratigraphy of the region (d) The depth of production and injection wells over the study area shown in Fig. 8-a.

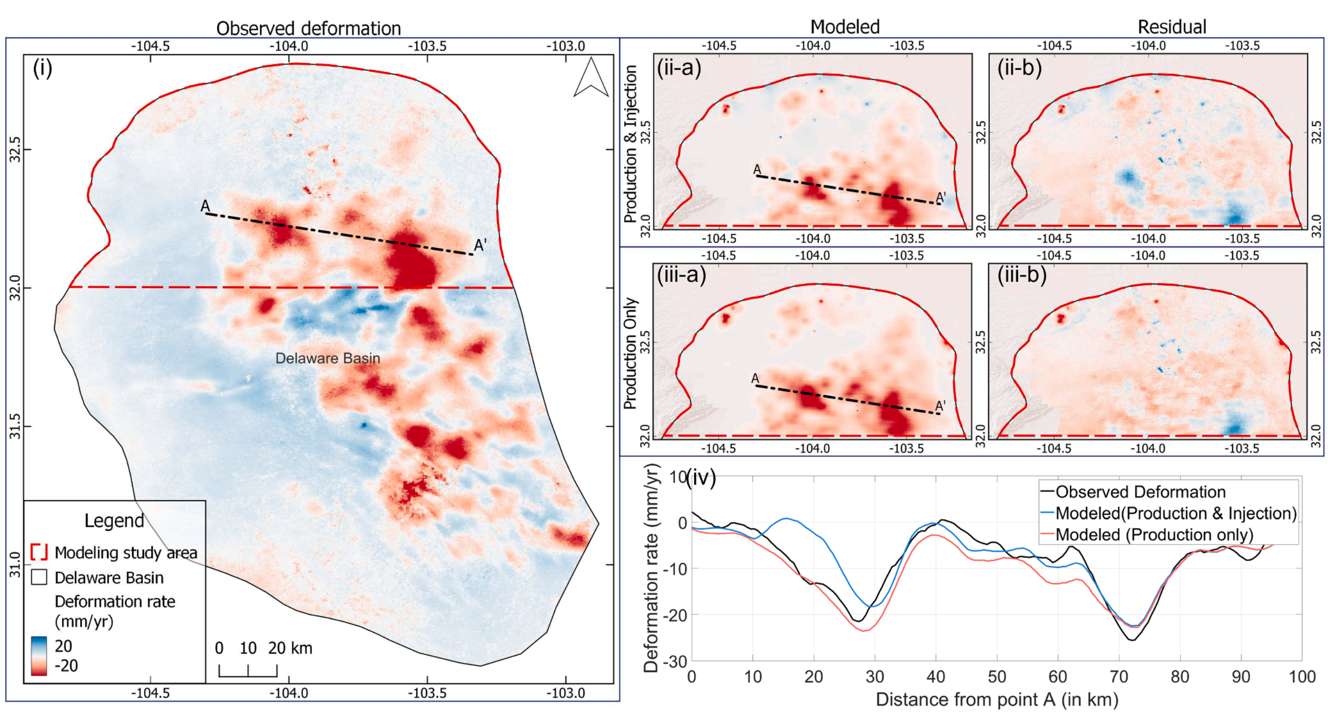

Fig. 8. (i) deformation rate (cm/yr) in the Delaware Basin between 2018 and 2021; (ii-a) deformation from distributed point source modeling of production and injection volumes and the (ii-b) deformation residual; (iii-a) deformation from distributed point source modeling of production volumes and the (ii-b) deformation residual; (iv) modeled and observed deformation in section profile A-A'.

(Fig. 6). The spatial extent of the deformation on the western part has not changed over the years even though the subsidence rate increased by up to 1 cm/yr coupled with the increase in the spatial extent on the eastern side. The horizontal deformation maps are also analyzed. The eastward deformation in the study area coincides with the shallow normal faults. A similar deformation pattern as the subsidence bowl α in Fig. 5(b) can be seen on the southeast side of Pecos City over the subsidence bowl β. While there are no mapped faults along the subsidence bowl β, the linear features on the western side hint at the presence of shallow normal faults in N-SE orientation similar to those along the subsidence bowl α. Another interesting deformation pattern can be seen from the profile C-C' (Fig. 6). Here we can observe a seesaw pattern in the deformation with several linear patterns of deformation seen close to each other. Here, the deformation rate is constant over the study period. While hydrocarbon extraction is the primary driver of this subsidence, it is key to note that the deformation is contained towards the north of the fault zone. Further, several such linear features are also observed along the Texas-New Mexico border over the regions experiencing uplift induced by shallow astewater injection. It is interesting to note that such examples exhibit the potential of InSAR in aiding fault identification in the Permian Basin. Pepin et al. (2022) and Staniewicz et al. (2020) have shown that the subsidence in the Southern Delaware Basin is linked to fault movement induced by fluid injection and extraction. The earthquake locations from the TexNet catalog shown above in Fig. 6(a&b) provide strength to the hypothesis. Earthquakes are clustered around the southern Delaware Basin in West Texas. Meanwhile, the development of a large subsidence bowl towards the north of GFZ during 2018-2021 can be observed in the deformation map (Fig. 6-b).

5.2. Deformation modeling

In the Northern Delaware Basin, in addition to no significant deformation along the identified fault lines, the subsidence does not show linear patterns, and little to no earthquake events are in the subsiding northern part hinting that the fault slip subsidence is absent in the region. This region is a part of the Lea and Eddy counties in New Mexico. These two counties are two of the top three oil and gas-producing counties in the Permian Basin. Here, primarily two subsidence bowls are identified with some localized subsidence patterns surrounding them subsiding at a rate of 3 cm/yr. The production data in the region is obtained and the production (hydrocarbon and produced water) and injection volumes are correlated with the land subsidence to find a matching pattern spatially as well as temporally (Fig. 7(b)). Thus, we have applied a distributed point source model considering each well as a deformation source. The average elevation of the study area is 1200 m above the mean sea level. The stratigraphy of the study area varies with the formations at higher depths towards the western side of the basin (Fig. 7(c)). In addition, formation thickness is slightly increasing towards the west. There are two major subsidence bowls over the study area with one subsidence bowl on the east side spread across 1250 sq km subsiding at a rate of 3 cm/yr and the one in the center spread across over 800 sq km subsiding at a rate of 2 cm/yr (Fig. 8(i)). In total, 10,315 producing wells and 580 injection wells active during the study period are chosen for the modeling (Fig. 7(a&d)). Most of the production wells are in the Bone spring Formation. While the injection is limited here, most of it is injected at deeper formations. The production wells are spread across the region except around the Potash mines and towards the western edge of the basin.

The surface deformation is modeled using the production and injection volumes, well locations, and depths. Poisson's ratio, ν is assumed to be 0.25. By inverting the observed deformation results, β is estimated as 0.28. Given both production and injection well data, the modeled deformation results agree with the observed except in two pockets (Fig. 8(ii-a)). When only production data is used for the modeling, the modeled deformation shows better agreement with the observed, especially in the interior of New Mexico (Fig. 8(iii-a)). The same can be observed from the graph in Fig. 8(iv): the deformation rates from the observed and the modeled largely agree in all cases with an average error rate of 0.2 cm/yr. But between 10 and 30 km in Fig. 8(iv), an uplift signal can be observed in the deformation modeled from production and injection data (red), while such a signal is absent from the observed results (black). Most of the injection in this area is taking place in the

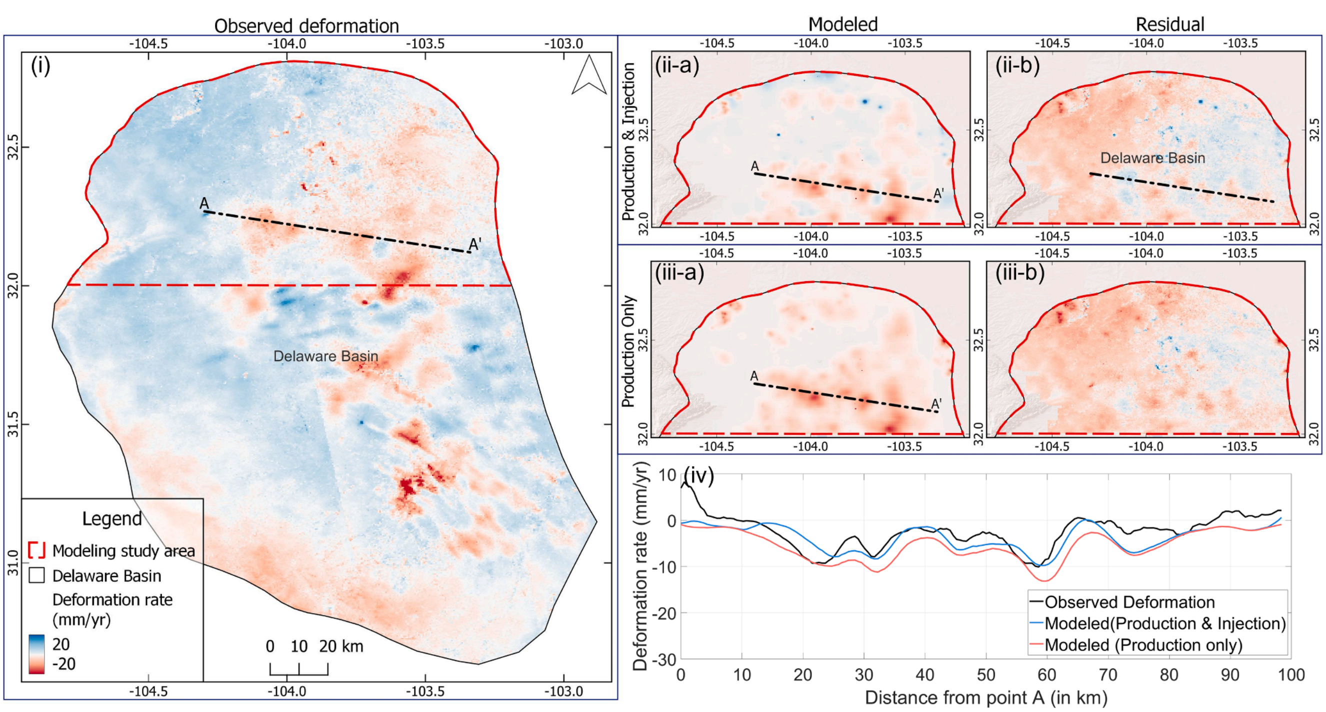

Fig. 9. (i) deformation rate (cm/yr) in the Delaware Basin between 2016 and 2017; (ii-a) deformation from distributed point source modeling of production and injection volumes and the (ii-b) deformation residual; (iii-a) deformation from distributed point source modeling of production volumes and the (ii-b) deformation residual; (iv) modeled and observed deformation in section profile A-A'.

deeper formations. Meanwhile, the residual along the Texas border is probably due to the diffused stress from production activities on the Texas side of the border. The modeling results suggest that the deep wastewater injection has minimal impact on surface deformation in the region. It is possible that the fluid pressure from the injected fluids was diffused southward over a large area and is manifested as the regional long-wavelength uplift observed in the Western Delaware Basin. This could be combined with another reason that due to years of continued production, the region has undergone inelastic deformation meaning that the initially subsided region has undergone permanent change and would not rebound even when a considerable volume of water is injected. Inelastic deformation occurs when the stress of the material exceeds the pre-consolidation stress (Smith & Li, 2021). Inelastic land surface deformation due to grain resettlement refers to the permanent changes in the shape and size of soil or sediment layers caused by the rearrangement of individual grains or particles due to excessive subsidence.

The remaining residual from the model is primarily in the central north portion. The hydrocarbon activity in this region is extremely limited due to the presence of potash mines and subsidence in the region is expected due to the mining operations and the salt dissolution. Potash mining in the Permian Basin can cause the collapse of the sedimentary rock layers above the mined-out areas, leading to subsidence and surface deformation. The rock layers above the mined-out areas can become unstable due to the removal of the potash deposits, creating voids or empty spaces underground. Over time, these voids can cause the overlying rock layers to shift and collapse, leading to subsidence at the ground surface. Sometimes, this can result in the formation of sinkholes and can pose a threat to not only the mining operations but also to the petroleum infrastructure such as pipelines and transportation networks. These cracks and sinkholes act as inlets for the rainwater into the subsurface resulting the salt dissolution which further aggravates the deformation in the region.

Further, this model was extended to the data from 2016 to 2017 (Fig. 9). The poroelasticity constant (β), is set as 0.28, as estimated from the previous results. The modeled results are generally consistent with the observed results. During this period, the hydrocarbon activities in the region were less intense than in the 2018–2021 period. This can also be reflected in the subsidence patterns over the region. The subsidence bowls are not developed by this time and the total subsiding area is nearly 1500 sq km subsiding at a rate of 1 cm/yr. The model can successfully reproduce much of the deformation to a 2 mm/yr accuracy similar to the previous results. When both production and injection data were used, a few localized uplift signals over the injection wells in the North-east part of the study area can be observed in the model. This signal is absent from the InSAR observations further confirming that the injection in the region is not reflected in the surface deformation. Interestingly, production in the North-West part of the study area along the Delaware Basin border is also not reflected in the surface deformation in both datasets. While the production here is carried out from deeper formations, it is important to consider the smaller formation thickness along the edges of the basin. As described earlier in the methodology section, a more detailed model taking the geology and poroelasticity into account is required to study such localized deformation signals. Further, during this period, a regional uplift signal can be observed over the western part of the study area. This signal is of a similar order of magnitude to the signal observed during 2018–2021. Considering that this signal is outside the shale play area with no significant hydrocarbon activities in the region, this deformation cannot be reproduced using the current model. Meanwhile, the injection and the associated uplift is limited during the 2016–2017 study period. Therefore, the response of the surface to the injection could not be explored. The other source of residual is from potash mining as explained above.

While we used an elastic model in this preliminary study, a more accurate study requires poroelastic modeling taking the surface deformation induced by fault slips, fluid flow obstruction by faults, pressure diffusion to larger distances, and other geologic processes into account to study the interaction between the solid subsurface and fluid hydrocarbons in detail. While this study is focused on the regional patterns of surface deformation in the Permian Basin, studying localized deformation in several areas is also crucial. Especially, the rapid subsidence events leading to the formation of sinkholes, deformation induced by the leakage of hydrocarbon fluids and wastewater, complex deformation patterns in the presence of faults, and horizontal migration of fluids are a few important concerns for the safe and stable hydrocarbon production in the region. Further, the data from various other sensors tracing back to 1991 such as ERS-1/2, ALOS-PALSAR, Envisat ASAR, and more can be used to study the evolution of the deformation in the Permian Basin in a more comprehensive way. When available, the new NISAR datasets (to be launched in 2024) provide a crucial input to the deformation maps to estimate the true 3D deformation by combining left (NISAR) and right (other SAR sensors) looking geometries. Considering the vast extent of the Permian Basin.

6. Conclusions

The Permian Basin, home to one of the largest oil reserves in the United States, is affected by surface deformation in several areas. First, the Delaware Basin is subsiding at a rate of up to 4 cm/yr between 2016 and 2021. In addition, several regions show an uplift of up to 2 cm/yr. Such differential settlements close to each other are a result of the rapid extraction of hydrocarbon fluids and the associated wastewater injection. The subsurface fluid flow can be altered by the presence of faults and thus, result in a complex surface deformation. The fault slips due to the pressure changes induced by the changes in the subsurface fluids can also pose a serious threat to the region's stability. Midland Basin has become increasingly important for hydrocarbon production over the last few years resulting in surface deformation. Several localized deformation patterns with subsidence and uplift are intertwined and can be observed in the Midland Basin. We have used advanced InSAR techniques to estimate the land subsidence and applied a scaled distributed point source modeling using the injection and production volume as well as the 3D well location data to understand the relation between the petroleum operations and the resulting land subsidence. The modeling results suggest that the injection into deep formations did not translate into surface deformation or that the region has undergone inelastic deformation. Future studies can consider the various geologic layers and their properties and the poroelastic principles to assess the subsidence more accurately by using more advanced finite element models. However, the inhomogeneity in the geologic properties over such a large region and the presence of thousands of oil wells may pose challenges in terms of the required processing time and the model's reliability.

Declaration of Competing Interest

The authors declare that they have no known competing financial interests or personal relationships that could have appeared to influence the work reported in this paper.

Data availability

Data will be made available on request.

Acknowledgment

This study was funded by NASA (National Aeronautics and Space Administration) Earth Surface and Interior Program (80NSSC21K1474) and NASA-ISRO SAR (NISAR) Science Team (80NSSC22K1888), and the Shuler-Foscue Endowment at Southern Methodist University.

Appendix A. Supplementary material

Supplementary data to this article can be found online at https://doi.org/10.1016/j.jag.2023.103424.

References

Bekaert, D.P.S., Hooper, A., Wright, T.J., 2015a. A spatially variable power law tropospheric correction technique for InSAR data. J. Geophys. Res. Solid Earth 120 (2), 1345–1356. https://doi.org/10.1002/2014JB011558.

Bekaert, D.P.S., Walters, R.J., Wright, T.J., Hooper, A.J., Parker, D.J., 2015b. Statistical comparison of InSAR tropospheric correction techniques. Remote Sens. Environ. 170, 40–47. https://doi.org/10.1016/j.rse.2015.08.035.

Bense, V.F., Person, M.A., 2006. Faults as conduit-barrier systems to fluid flow in siliciclastic sedimentary aquifers. Water Resour. Res. 42 (5) https://doi.org/10.1029/2005WR004480.

Blewitt, G., Hammond, W., Kreemer, C., 2018. Harnessing the GPS Data Explosion for Interdisciplinary Science. Eos 99. https://doi.org/10.1029/2018EO104623.

Caine, J.S., Forster, C.B., 1999. Fault zone architecture and fluid flow: Insights from field data and numerical modeling. In: Haneberg, W.C., Mozley, P.S., Moore, J.C., Goodwin, L.B. (Eds.), Geophysical Monograph Series, Vol. 113. American Geophysical Union, pp. 101–127. https://doi.org/10.1029/GM113p0101.

Crosetto, M., Monserrat, O., Cuevas-González, M., Devanthéry, N., Crippa, B., 2016. Persistent Scatterer Interferometry: A review. ISPRS J. Photogramm. Remote Sens. 115, 78–89. https://doi.org/10.1016/j.isprsjprs.2015.10.011.

Copernicus Sentinel Data. (2016, 2022). Alaska Satellite Facility.

Denlinger, R.P., O'Connell, R.H., D., 2020. Evolution of Faulting Induced by Deep Fluid Injection, Paradox Valley, Colorado. Bull. Seismol. Soc. Am. 110 (5), 2308–2327. https://doi.org/10.1785/0120190328.

Dhakal, S., Minx, J. C., Toth, F. L., Abdel-Aziz, A., Figueroa Meza, M. J., Hubacek, K., Jonckheere, I. G. C., Kim, Y.-G., Nemet, G. F., Pachauri, S., Tan, X. C., & Wiedmann, T. (2022). Emissions Trends and Drivers. In P. R. Shukla, J. Skea, R. Slade, A. A. Khourdajie, R. van Diemen, D. McCollum, M. Pathak, S. Some, P. Vyas, R. Fradera, M. Belkacemi, A. Hasija, G. Lisboa, S. Luz, & J. Malley (Eds.), *IPCC, 2022: Climate Change 2022: Mitigation of Climate Change. Contribution of Working Group III to the Sixth Assessment Report of the Intergovernmental Panel on Climate Change*. Cambridge University Press. https://doi.org/10.1017/9781009157926.004.

Drouin, V., Sigmundsson, F., 2019. Countrywide Observations of Plate Spreading and Glacial Isostatic Adjustment in Iceland Inferred by Sentinel-1 Radar Interferometry, 2015–2018. Geophys. Res. Lett. 46 (14), 8046–8055. https://doi.org/10.1029/2019GL082629.

Ellsworth, W.L., 2013. Injection-Induced Earthquakes. 341 (July), 1–8.

Ferretti, A., Fumagalli, A., Novali, F., Prati, C., Rocca, F., Rucci, A., 2011. A new algorithm for processing interferometric data-stacks: SqueeSAR. IEEE Trans. Geosci. Remote Sens. 49 (9), 3460–3470. https://doi.org/10.1109/TGRS.2011.2124465.

Frohlich, C., DeShon, H., Stump, B., Hayward, C., Hornbach, M., Walter, J.I., 2016. A Historical Review of Induced Earthquakes in Texas. Seismol. Res. Lett. 87 (4), 1022–1038. https://doi.org/10.1785/0220160016.

Garg, S., Motagh, M., Indu, J., Karanam, V., 2022. Tracking hidden crisis in India's capital from space: Implications of unsustainable groundwater use. Sci. Rep. 12 (1), 651. https://doi.org/10.1038/s41598-021-04193-9.

Hennings, P., Dvory, N., Horne, E., Li, P., Savvaidis, A., Zoback, M., 2021. Stability of the Fault Systems That Host-Induced Earthquakes in the Delaware Basin of West Texas and Southeast New Mexico. The Seismic Record 1 (2), 96–106. https://doi.org/10.1785/0320210020.

Hooper, A.J., 2008. A multi-temporal InSAR method incorporating both persistent scatterer and small baseline approaches. Geophys. Res. Lett. 35 (16), 1–5. https://doi.org/10.1029/2008GL034654.

Hooper, A., Zebker, H., Segall, P., Kampes, B., 2004. A new method for measuring deformation on volcanoes and other natural terrains using InSAR persistent scatterers. Geophys. Res. Lett. 31 (23) https://doi.org/10.1029/2004GL021737.

Horne, E. A., Hennings, P. H., & Zahm, C. K. (2021). Basement-Rooted Faults of the Delaware Basin and Central Basin Platform, Permian Basin, West Texas and Southeastern New Mexico. In *The geologic basement of Texas: A volume in honor of Peter T. Flawn* (Vol. 286, Issue 286). https://doi.org/10.23867/RI0286C6.Copyright.

Intrepid Potash, I.P., 2016. Intrepid Potash Announces the Idling of its West Facility; Takes Next Step in Business Transformation. Intrepid Potash. https://archive.is/0wWYJ.

Jones, N.F., Pejchar, L., Kiesecker, J.M., 2015. The Energy Footprint: How Oil, Natural Gas, and Wind Energy Affect Land for Biodiversity and the Flow of Ecosystem Services. Bioscience 65 (3), 290–301. https://doi.org/10.1093/biosci/biu224.

Joshi, M., Kothyari, G.C., Kotlia, B.S., 2023. Landslide detection in Kinnaur Valley, NW India using PS-InSAR technique. Phys. Geogr. 1–15 https://doi.org/10.1080/02723646.2023.2202932.

Kandregula, R.S., Kothyari, G.C., Swamy, K.V., Kumar Taloor, A., Lakhote, A., Chauhan, G., Thakkar, M.G., Pathak, V., Malik, K., 2022. Estimation of regional surface deformation post the 2001 Bhuj earthquake in the Kachchh region, Western India using RADAR interferometry. Geocarto Int. 37 (18), 5249–5277. https://doi.org/10.1080/10106049.2021.1899299.

Karanam, V., Motagh, M., Garg, S., Jain, K., 2021. Multi-sensor remote sensing analysis of coal fire induced land subsidence in Jharia Coalfields, Jharkhand, India. Int. J. Appl. Earth Obs. Geoinf. 102, 102439 https://doi.org/10.1016/j.jag.2021.102439.

Ketelaar, V. B. H. (2009). Satellite Radar Interferometry (Vol. 14). Springer Netherlands. https://doi.org/10.1007/978-1-4020-9428-6.

Kim, J., Coe, J.A., Lu, Z., Avdievitch, N.N., Hults, C.P., 2022. Spaceborne InSAR mapping of landslides and subsidence in rapidly deglaciating terrain, Glacier Bay National Park and Preserve and vicinity, Alaska and British Columbia. Remote Sens. Environ. 281, 113231 https://doi.org/10.1016/j.rse.2022.113231.

Kim, J.W., Lu, Z., 2018. Association between localized geohazards in West Texas and human activities, recognized by Sentinel-1A/B satellite radar imagery. Sci. Rep. 8 (1), 1–13. https://doi.org/10.1038/s41598-018-23143-6.

Kim, J.-W., Lu, Z., Kaufmann, J., 2019. Evolution of sinkholes over Wink, Texas, observed by high-resolution optical and SAR imagery. Remote Sens. Environ. 222, 119–132. https://doi.org/10.1016/j.rse.2018.12.028.

Liu, Y., Huang, H., Liu, Y., Bi, H., 2016. Linking land subsidence over the Yellow River delta, China, to hydrocarbon exploitation using multi-temporal InSAR. Nat. Hazards 84 (1), 271–291. https://doi.org/10.1007/s11069-016-2427-5.

Lu, Z., & Dzurisin, D. (2014). InSAR Imaging of Aleutian Volcanoes. In Z. Lu & D. Dzurisin, *InSAR Imaging of Aleutian Volcanoes* (pp. 87–345). Springer Berlin Heidelberg. https://doi.org/10.1007/978-3-642-00348-6_6.

Lu, Z., Danskin, W.R., 2001. InSAR analysis of natural recharge to define structure of a ground-water basin, San Bernardino. California. *Geophysical Research Letters* 28 (13), 2661–2664. https://doi.org/10.1029/2000GL012753.

Lu, Z., Masterlark, T., Power, J., Dzurisin, D., Wicks, C., 2002. Subsidence at Kiska Volcano, Western Aleutians, detected by satellite radar interferometry: InSAR study of Kiska volcano, Alaska. Geophys. Res. Lett. 29 (18), 2-1–2-4. https://doi.org/10.1029/2002GL014948.

Mishra, V., Jain, K., 2022. Satellite based assessment of artificial reservoir induced landslides in data scarce environment: A case study of Baglihar reservoir in India. J Appl Geophy 205, 104754. https://doi.org/10.1016/j.jappgeo.2022.104754.

Mogi, K., 1958. Relations of the eruptions of various volcanoes and the deformations of the ground around them. Bull. Earthq. Res. Inst. Tokyo Univ 36, 98–134.

Pepin, K.S., Ellsworth, W.L., Sheng, Y., Zebker, H.A., 2022. Shallow Aseismic Slip in the Delaware Basin Determined by Sentinel-1 InSAR. *Journal of Geophysical Research: Solid.* Earth. https://doi.org/10.1029/2021JB023157.

Popova, O., 2020a. *Wolfcamp and Spraberry Shale Plays of the Midland Basin: Geology review* (Permian Basin). United States Energy Information Administration. https://www.eia.gov/maps/pdf/EIA-Permian-Part-II.pdf.

Popova, O., 2020b. *Wolfcamp, Bone Spring, Delaware Shale Plays of the Delaware Basin: Geology review* (Permian Basin). United States Energy Information Administration. https://www.eia.gov/maps/pdf/Permian-pI_Wolfcamp-Bonespring-Delaware.pdf.

Popova, O., & Long, G. (2022, September 30). *Advances in technology led to record new well productivity in the Permian Basin in 2021*. US Energy Information Administration. https://www.eia.gov/todayinenergy/detail.php?id=54079#.

Qu, F., Lu, Z., Kim, J.-W., Zheng, W., 2019. Identify and Monitor Growth Faulting Using InSAR over Northern Greater Houston, Texas, USA. Remote Sens. (Basel) 11 (12), 1498. https://doi.org/10.3390/rs11121498.

Savvaidis, A., Lomax, A., Breton, C., 2020. Induced Seismicity in the Delaware Basin, West Texas, is Caused by Hydraulic Fracturing and Wastewater Disposal. Bull. Seismol. Soc. Am. 110 (5), 2225–2241. https://doi.org/10.1785/0120200087.

Savvaidis, A. (2021). *TexNet High Resolution Earthquake Catalog*. https://doi.org/10.15781/76HJ-ED46.

Shi, J., Xu, B., Chen, Q., Hu, M., Zeng, Y., 2022. Monitoring and analysing long-term vertical time-series deformation due to oil and gas extraction using multi-track SAR dataset: A study on lost hills oilfield. Int. J. Appl. Earth Obs. Geoinf. 107, 102679 https://doi.org/10.1016/j.jag.2022.102679.

Smith, R., Li, J., 2021. Modeling elastic and inelastic pumping-induced deformation with incomplete water level records in Parowan Valley, Utah. J. Hydrol. 601, 126654 https://doi.org/10.1016/j.jhydrol.2021.126654.

Snee, J.E.L., Zoback, M.D., 2018. State of stress in the Permian Basin, Texas and New Mexico: Implications for induced seismicity. Leading Edge 37 (2), 127–134. https://doi.org/10.1190/tle37020127.1.

Staniewicz, S., Chen, J., Lee, H., Olson, J., Savvaidis, A., Reedy, R., Breton, C., Rathje, E., Hennings, P., 2020. InSAR Reveals Complex Surface Deformation Patterns Over an 80,000 km 2 Oil-Producing Region in the Permian Basin. Geophys. Res. Lett. 47 (21) https://doi.org/10.1029/2020GL090151.

USEIA. (2023, January 17). Permian Region Drilling Productivity Report. U. S. Energy Information Administration. https://www.eia.gov/petroleum/drilling/pdf/permian.pdf.

Wright, T., Parsons, B., Fielding, E., 2001. Measurement of interseismic strain accumulation across the North Anatolian Fault by satellite radar interferometry. Geophys. Res. Lett. 28 (10), 2117–2120. https://doi.org/10.1029/2000GL012850.

Yu, C., Li, Z., Penna, N.T., Crippa, P., 2018. Generic Atmospheric Correction Model for Interferometric Synthetic Aperture Radar Observations. J. Geophys. Res. Solid Earth 123 (10), 9202–9222. https://doi.org/10.1029/2017JB015305.

Zhai, G., Shirzaei, M., Manga, M., 2021. Widespread deep seismicity in the Delaware Basin, Texas, is mainly driven by shallow wastewater injection. Proc Natl Acad Sci U S A 118 (20), 1–7. https://doi.org/10.1073/pnas.2102338118.

Zhang, A., Lu, J., Kim, J.-W., 2018. Detecting mining-induced ground deformation and associated hazards using spaceborne InSAR techniques. Geomat. Nat. Haz. Risk 9 (1), 211–223. https://doi.org/10.1080/19475705.2017.1415229.

Zheng, W., Hu, J., Lu, Z., Hu, X., Sun, Q., Liu, J., Zhu, J., Li, Z., 2023. Enhanced Kinematic Inversion of 3-D Displacements, Geometry, and Hydraulic Properties of a North-South Slow-Moving Landslide in Three Gorges Reservoir. J. Geophys. Res. Solid Earth, e2022JB026232. https://doi.org/10.1029/2022JB026232.

Zheng, W., Kim, J.-W., Ali, S.T., Lu, Z., 2019. Wastewater leakage in West Texas revealed by satellite radar imagery and numerical modeling. Sci. Rep. 9 (1), 14601. https://doi.org/10.1038/s41598-019-51138-4.